Title

Towards characterization of photo-excited electron transfer and catalysis in natural and artificial systems using XFELs

Authors

Alonso-Mori, R
Asa, K
Bergmann, U
et al.

Publication Date

2016-12-16

DOI

10.1039/c6fd00084c

Peer reviewed

Faraday Discussions

Cite this: *Faraday Discuss.*, 2016, **194**, 621

Towards characterization of photo-excited electron transfer and catalysis in natural and artificial systems using XFELs

R. Alonso-Mori,[a] K. Asa,[b] U. Bergmann,[c] A. S. Brewster,[d] R. Chatterjee,[d] J. K. Cooper,[e] H. M. Frei,[d] F. D. Fuller,[d] E. Goggins,[f] S. Gul,[d] H. Fukuzawa,[gh] D. Iablonskyi,[g] M. Ibrahim,[i] T. Katayama,[j] T. Kroll,[k] Y. Kumagai,[g] B. A. McClure,[d] J. Messinger,[l] K. Motomura,[gh] K. Nagaya,[bh] T. Nishiyama,[b] C. Saracini,†[d] Y. Sato,[b] N. K. Sauter,[d] D. Sokaras,[k] T. Takanashi,[g] T. Togashi,[j] K. Ueda,[gh] W. W. Weare,[f] T.-C. Weng,[m] M. Yabashi,[j] V. K. Yachandra,[d] I. D. Young,[d] A. Zouni,[i] J. F. Kern*[ad] and J. Yano*[deg]

Received 18th April 2016, Accepted 2nd June 2016
DOI: 10.1039/c6fd00084c

The ultra-bright femtosecond X-ray pulses provided by X-ray Free Electron Lasers (XFELs) open capabilities for studying the structure and dynamics of a wide variety of biological and inorganic systems beyond what is possible at synchrotron sources. Although the structure and chemistry at the catalytic sites have been studied intensively in both biological and inorganic systems, a full understanding of the atomic-scale chemistry requires new approaches beyond the steady state X-ray crystallography and X-ray spectroscopy at cryogenic temperatures. Following the dynamic changes in the

[a]*Linac Coherent Light Source, SLAC National Accelerator Laboratory, Menlo Park, CA 94025, USA*
[b]*Department of Physics, Graduate School of Science, Kyoto U., Kyoto, 606-8502, Japan*
[c]*Stanford PULSE Institute, SLAC National Accelerator Laboratory, Menlo Park, CA 94025, USA*
[d]*Molecular Biophysics and Integrated Bioimaging Division, Lawrence Berkeley National Laboratory, 1 Cyclotron Rd., Berkeley, CA 94720, USA. E-mail: JFKern@lbl.gov; JYano@lbl.gov*
[e]*Joint Center for Artificial Photosynthesis (JCAP), Lawrence Berkeley National Laboratory, 1 Cyclotron Rd., Berkeley, CA 94720, USA*
[f]*Dept. of Chemistry, North Carolina State University, 2620 Yarborough Rd., Raleigh, NC 27695-8204, USA*
[g]*IMRAM, Tohoku U., Sendai 980-8577, Japan*
[h]*RIKEN SPring-8 Center, Kouto, Sayo, Hyogo 679-5148, Japan*
[i]*Institut für Biologie, Humboldt-Universität zu Berlin, D-10099 Berlin, Germany*
[j]*Japan Synchrotron Radiation Research Institute (JASRI), SPring-8/SACLA, Kouto, Sayo-cho, Sayo-gun, Hyogo 679-5198, Japan*
[k]*Stanford Synchrotron Radiation Lightsource (SSRL), SLAC National Accelerator Laboratory, Menlo Park, CA 94025, USA*
[l]*Institutionen för Kemi, Kemiskt Biologiskt Centrum, Umeå Universitet, Umeå, Sweden*
[m]*Center for High Pressure Science & Technology Advanced Research, Shanghai, China*
† Current address: Center for Biomimetic Systems (CBS), Ewha Womans University, Department of Bioinspired Science, Seoul, 120-750, Korea.

geometric and electronic structure at ambient conditions, while overcoming X-ray damage to the redox active catalytic center, is key for deriving reaction mechanisms. Such studies become possible by using the intense and ultra-short femtosecond X-ray pulses from an XFEL, where sample is probed before it is damaged. We have developed methodology for simultaneously collecting X-ray diffraction data and X-ray emission spectra, using an energy dispersive spectrometer, at ambient conditions, and used this approach to study the room temperature structure and intermediate states of the photosynthetic water oxidizing metallo-protein, photosystem II. Moreover, we have also used this setup to simultaneously collect the X-ray emission spectra from multiple metals to follow the ultrafast dynamics of light-induced charge transfer between multiple metal sites. A Mn–Ti containing system was studied at an XFEL to demonstrate the efficacy and potential of this method.

1. Introduction

Many of the catalytic reactions in inorganic systems and natural enzymes involve multiple electrons, and proceed through several intermediate steps. For example, photosynthetic water oxidation in nature is catalyzed by an oxo-bridged Mn_4Ca metal center located in a multi-subunit membrane protein, photosystem II (PS II) (Fig. 1). An understanding of the mechanism of light-harvesting, charge separation and catalysis is well-connected to the function of this molecular machine. A PS II monomer consists of 17 or 18 membrane integral subunits composed of 35–36 *trans*-membrane helices and 3 peripheral subunits. In addition, there are many cofactors, 35 chlorophyll a (Chl), 11–12 all-*trans* β-carotene molecules, 1 OEC (Oxygen Evolving Complex, Mn_4CaO_5 cluster), 1 heme b, one heme c, 2 or 3 plastoquinones, 2 pheophytins, and 1 nonheme Fe, that are important for light-harvesting, charge separation and stabilization, and electron transfer. The high-

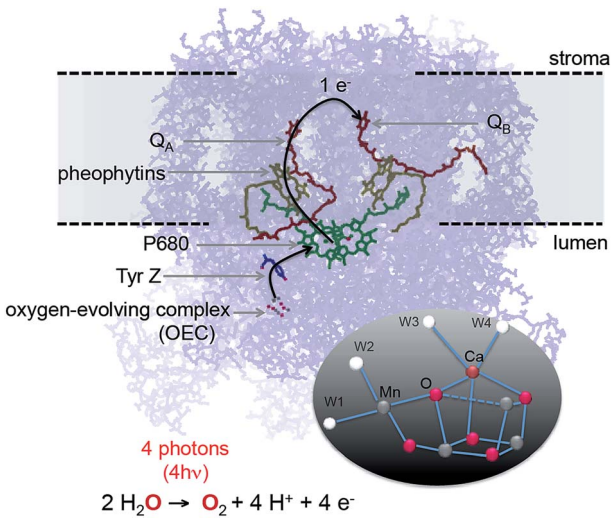

Fig. 1 The electron transfer chain of photosystem II. The inset shows the structure of the water oxidizing Mn_4CaO_5 catalyst.[1]

resolution X-ray crystal structures of PS II from a thermophilic cyanobacterium has been reported to a resolution of 1.9 Å, revealing the detailed architecture of this enzyme.[1,2]

In parallel to the basic understanding of natural enzymes, learning from natural systems on how to control electron flow between multiple sites that can undergo an ultrafast photo-excited charge separation is a key issue for developing materials such as artificial photosynthetic devices and magnetic materials. For example, a rapid charge separation in inorganic chromophores is often accomplished *via* a metal-to-metal charge transfer event (MMCT). To be useful for driving a multi-electron catalyst, as required for processes such as CO_2 reduction or water oxidation, the excited state that is formed by the initial ultrafast processes in the binuclear charge transfer unit has to be sufficiently long lived to allow for electron transport to/from the catalyst. To understand such sequential chemistry, it is important to probe signals from multiple metal sites simultaneously in a time-resolved manner.

The introduction of X-ray Free Electron Lasers (XFELs) has made it possible to follow photochemical reactions in biological systems at room temperature, using time-resolved detection methods, before the onset of radiation-induced changes propagates, by taking advantage of the ultrashort femtosecond X-ray pulses. Similarly, detecting early picosecond to sub picosecond time-scale phenomena using X-ray techniques has become possible, expanding the impact of such photochemical studies to many inorganic systems with ultrafast excited state dynamics.

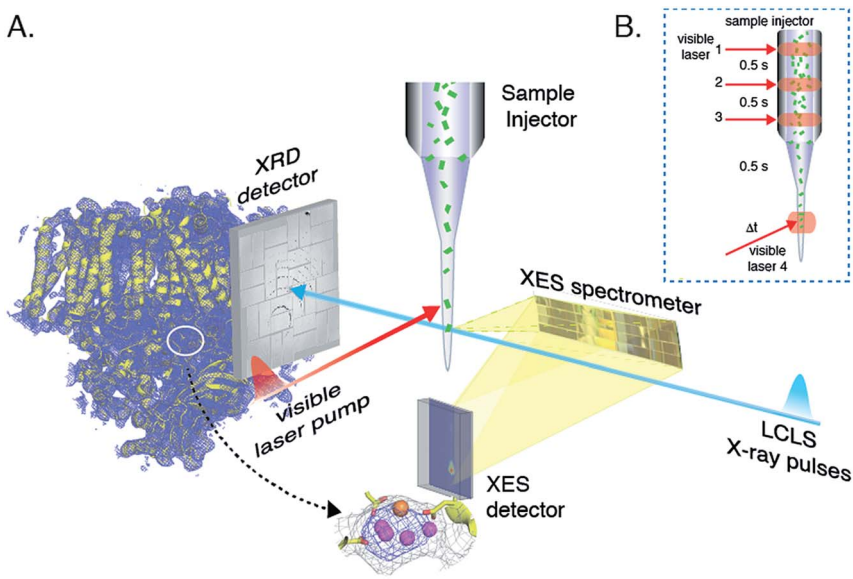

Fig. 2 (A) Simultaneous collection of X-ray diffraction data (downstream) providing overall structural information and X-ray emission spectra (at 90 degrees) using the wavelength-dispersive spectrometer providing electronic structure information of the metal site.[3,4] Adapted from Kern *et al.*[5] (B) Multiple illumination protocol used for triggering photochemical reactions that can be probed using the femtosecond X-ray pulses from the XFEL.

We have developed several X-ray-based techniques suitable for studying photochemical reactions in biological and inorganic systems at XFEL facilities (XFELs).[3–8] Fig. 2 shows a wavelength-dispersive X-ray emission spectrometer that has been developed and used for collecting X-ray emission spectra (XES) at the LCLS (Linac Coherent Light Source, SLAC, USA) and SACLA (Spring 8, Japan). This setup is suitable for shot-by-shot data collection at XFELs, as it can collect the entire emission spectrum at once. It also has several advantages for dealing with the inherent properties of the XFELs, *e.g.* it does not require a beamline monochromator and it is compatible with the XFEL SASE (Self-Amplified Spontaneous Emission) spectral profile in which the energy bandwidth is 0.2–0.5% (FWHM) of the total SASE energy for hard X-rays. In addition, the shot-by-shot variation of the intensity and the energy distribution of the SASE beam is not an issue. Wavelength-dispersive XES can also be combined with other techniques like crystallography in which the same incoming X-rays can be used for simultaneous collection of the diffraction (XRD) signal to obtain complementary structural information. Moreover, this setup allows detecting emission signals from multiple elements simultaneously, which is useful to follow the time-course of sequential reactions in multimetallic sites in biological and inorganic systems.

In this work, we present the XES and related methodology we have developed at XFELs and its application to study photochemical reactions in both biological and inorganic systems.

2. Photochemically driven electron transfer and the water oxidation reaction in photosystem II

A. Photosystem II

In Fig. 1, the electron transfer chain in PS II is shown, where light-harvesting, charge separation, charge stabilization, and electron transfer take place. The P_{680} (an ensemble of up to 4 chlorophyll and 2 pheophytin molecules that are excitonically coupled) located in the D1 and D2 subunits is the primary electron donor that traps the light energy delivered from the inner antenna subunits (CP43 and CP47 subunits) or the outer antenna complexes (LHC1 and LHC2) of PS II. The excited state of the primary donor P_{680}^{*} rapidly transfers the electron to Chl_{D1}, pheophytin ($Pheo_{D1}$) and subsequently to the acceptor, plastoquinone Q_A (a firmly bound plastoquinone) and ultimately to the final electron acceptor plastoquinone Q_B, stabilizing the charge-separated state. After accepting two electrons from the Mn_4CaO_5 cluster and after protonation the acceptor Q_B becomes plastoquinol $QH_{2(B)}$, which is released from PS II into the membrane matrix for transfer to the $cytb_6f$ complex. The latter connects the electron transfer chain between PS II and PS I. On the donor end of PS II, the cationic Chl radical $P_{680}^{\bullet+}$ is reduced by a tyrosine residue, Tyr_Z (D1Tyr161), to generate a neutral tyrosine radical $Tyr_Z^{\bullet}$ which acts as an oxidant for the water oxidation process at the OEC (see also Fig. 3 in the later section).

The OEC cycles through a series of five intermediate S-states (S_i, $i = 0$ to 4), representing the number of oxidizing equivalents stored in the OEC driven by the energy of the four successive photons absorbed by the PS II reaction center (see Fig. 4 in the later section).[9] When PS II is dark-adapted, it relaxes to the S_1 state

(note that although S_0 is the most reduced state of the OEC, the S_0 state is oxidized by tyrosine D(Y_D^{*+}) during the dark adaptation and therefore the S_1 state becomes the dark-stable state). Illumination of dark-adapted PS II (the S_1 state) with saturating flashes of visible light leads to a maximum O_2 yield after the 3rd flash, and then after every 4th successive flash. Each flash advances the oxidation state of the OEC by removing one electron, and the OEC acts like a redox capacitor for the water oxidation reaction until the four oxidizing equivalents are accumulated (S_4-state). Once four oxidizing equivalents are accumulated in the OEC, a spontaneous reaction occurs that results in the oxidation of water, release of O_2 and the formation of the S_0-state. Thus, the Mn_4CaO_5 complex in the OEC couples the four-electron four-proton oxidation of water with the one-electron photochemistry occurring at the PS II reaction center by acting as the locus of charge accumulation.[10]

During the reaction, the Mn cluster provides a high degree of redox and chemical flexibility, while protein residues are critical for mediating the reaction by modulating redox potentials and providing pathways for electrons, protons, substrate H_2O, and product O_2.[11,12] Thus, PS II orchestrates a well-controlled catalytic reaction at close to the thermodynamic potential, while avoiding the release of chemical intermediate species, such as superoxide or peroxide, during the water oxidation reaction that can be detrimental to the protein matrix and to the chemistry occurring at the OEC.

To follow catalysis under physiological conditions in PS II, X-ray crystallography and X-ray spectroscopy methods have been used at XFELs.[5] In particular, the simultaneous collection of crystallography and X-ray spectroscopy data has been proven to be a powerful method for studying metalloenzymes like PS II (Fig. 2), providing important insights from both the atomic structure of the protein crystals and the emission signals from the metal catalytic centers. This setup allows accessing time resolved data during photochemical reactions triggered using visible light.

B. Room temperature crystallography and spectroscopy of PS II

XFEL serial femtosecond X-ray crystallography has been proven to be a new way of doing protein crystallography.[13] In general, biological crystallography at a synchrotron facility is carried out at cryogenic temperatures to minimize the radiation-induced changes during data collection, summarized as radiation damage.[14] Nevertheless, in the case of metalloenzymes, often damage to the active site is observed even under cryogenic conditions and at a dose well below the dose threshold leading to an observable loss of diffractivity.[15–17] It is accepted that the cooling process, typically to 100–150 K, does not perturb the functional structure of enzymes. However, it is also known that the temperature could shift the intrinsic population of conformers in many proteins.[18–20] Protein dynamics play a critical role in enzymatic functions, and therefore many enzymes do not function at freezing temperatures. For some systems, the conformational landscape that is important for enzyme function may not be captured under cryo-cooled conditions. In addition, data collection at cryogenic temperatures can prevent capturing short-lived reactive intermediates unless such species can be cryo-trapped within the time-scale of state-of the art freeze-quenching methods. Thus, data collection under physiological conditions is required in such cases.

We have collected room temperature X-ray diffraction data from PS II at the CXI instrument[21,22] at the LCLS using 9.5 keV incident X-rays. The rmsd (root-mean-square deviation) of the room temperature dark state crystal structure of PS II in comparison with the cryogenic structure of the same protein reported by Suga *et al.*[1] showed that the changes are mostly within 2 Å, and they are in the solvent-exposed region of the protein. This implies that the cofactor distances in the electron transfer chain remain similar to those obtained at cryogenic temperature, as the cofactors are present in the hydrophobic interior of the PS II membrane complex.

In terms of the chemical states of the Mn_4CaO_5 catalytic center in PS II, a similar XES spectrum in the dark state was observed in both XFEL room temperature and synchrotron cryogenic temperature data.[5] This evidence demonstrates that the catalytic center at room temperature remains intact under the XFEL data collection conditions used in this study. The XES data also serves as a diagnostic tool for evaluating the chemical state of the samples.[23]

C. S-State advancement and acceptor side chemistry

The dark S_1 state can be advanced to higher S-states with a laser flash(es) at room temperature. By cryo-trapping the sample after the laser flash, each S-state (S_0, S_2, S_3, in addition to the dark S_1 state) has been characterized at synchrotron X-ray facilities. As the S-states do not decay rapidly, freeze-quenching of the illuminated samples to liquid N_2 temperature within a couple of seconds is sufficient for trapping the stable intermediates like S_2, S_3, and S_0 states. The yield is never 100% due to the intrinsic limitations in PS II S-state advancement because of misses and double-hits by visible light photons. In the best case, a S-state distribution after each flash is similar to what is shown in the inset table in Fig. 3. The $T_{1/2}$ of each S-state has been obtained from the literature,[24–26] and also summarized in this figure.

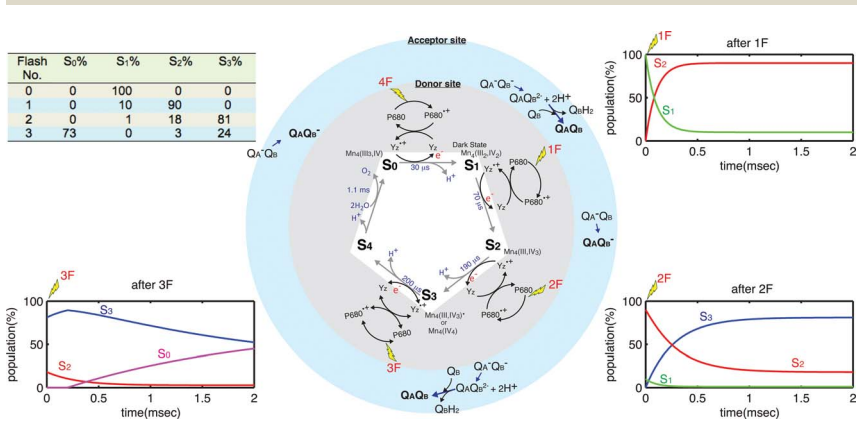

Fig. 3 Center: The Kok S-state cycle for water oxidation by PS II. Gray – donor side: each of the four photons absorbed by the PS II P_{680} reaction center oxidizes the tyrosine Y_Z intermediate, which in turn oxidizes the Mn_4CaO_5 complex. Blue – acceptor side: Q_A and Q_B are reduced on the acceptor side. Left top: A best case steady state S-state population as a function of laser-flash illuminations. 10% miss hit is assumed. Insets: The evolution of the populations of the S-states as a function of time are shown after 1flash (1F), 2 flashes (2F) and 3 flashes (3F).[24–26]

Stable charge separation is the prerequisite for advancing the Mn_4CaO_5 cluster of the oxygen-evolving complex (OEC) from one oxidation state to the next higher one. It is well known that stable charge separation can only be achieved if the acceptor quinone, Q_A, is present in the oxidized state (Fig. 3).[27] It is thus impossible to uncouple the S state advancement from the often slower acceptor side kinetics, *i.e.* the electron transfer from Q_A^- to Q_B or Q_B^-, and the formation and exchange of Q_BH_2 with a plastoquinone molecule from the thylakoid membrane (or a pre-bound Q_C molecule).[28,29] Thus, an important parameter governing the yield of the S_3 state after two flashes is the amount of open centers (Q_A) at the time point of the second flash. A stable charge separation can only happen in centers where Q_A is present in the oxidized form (see *e.g.* ref. 27), whereas in closed centers only a very small fraction (<10%) can proceed to the next higher S-state. If the second light excitation flash is given in the earlier stage after the first flash, a large fraction of the centers still have reduced Q_A (Q_A^-) and are thus closed, meaning they cannot produce a stable $P_{680}^{\bullet+}$ to advance the Mn_4CaO_5 cluster from the S_2 into the S_3 state. To establish the illumination conditions at XFELs, a replica of the XFEL illumination set up was built to study the advancement of the sample using isotope labeling and membrane inlet mass spectrometry (MIMS) under practically identical conditions as at the beamline. Optimization of all these parameters is absolutely crucial for achieving optimal sample turnover with a low miss factor.

The electron transfer rate between Q_A^- and Q_B or Q_B^-, and the exchange rate of Q_BH_2 with PQ, are species- and sample-dependent. We thus measured the time scale of such electron transfer events in the preparations used for our experiments. The fastest rates reported so far is by de Wijn & van Gorkom[30] for spinach membrane fragments. We note that measurements on intact cells show that wait-times between flashes in the order of 10's to 100's of ms are necessary to ensure turnover of the OEC and the acceptor side.[31] The S-state advancement in crystals should not be fundamentally different from all the literature values available.

We have collected the 2F XRD and XES data at CXI at LCLS using conditions similar to those described in the previous section. The dark-adapted PS II sample was illuminated *in situ* with 532 nm visible laser light (2 flashes) with the setup shown in Fig. 2, by turning-on fiber-coupled lasers 2 and 3. Incident X-rays of 9.5 keV were used for the experiment. Fig. 4A shows the Mn XES $K\beta_{1,3}$ peak shift observed between the dark (0F) and 2F data. The $K\beta_{1,3}$ transition of Mn corresponds to a fluorescence decay of 3p to 1s orbitals, that occurs after the excitation of the 1s core electron to the continuum. Similar difference spectra were observed for the synchrotron (cryogenic) and the XFEL (room temperature) data, indicating that the S-state advancement under our experimental conditions was comparable to that of samples prepared by the freeze-quenching method for synchrotron experiments.[3] The same setup was used to collect the XRD data of the 2F sample, and the data has been published.[23]

As mentioned above, the simultaneous collection of crystallography and X-ray spectroscopy data using crystalline samples is a valuable approach for studying the overall protein structure together with the chemistry that occurs at the metal catalytic centers. XES can also be used for diagnostic purposes during XRD data collection to ensure the intactness of the metal catalytic centers. However, some caution is necessary when crystallography and spectroscopic data are collected under the same conditions. Fig. 4B shows a single-shot diffraction pattern from

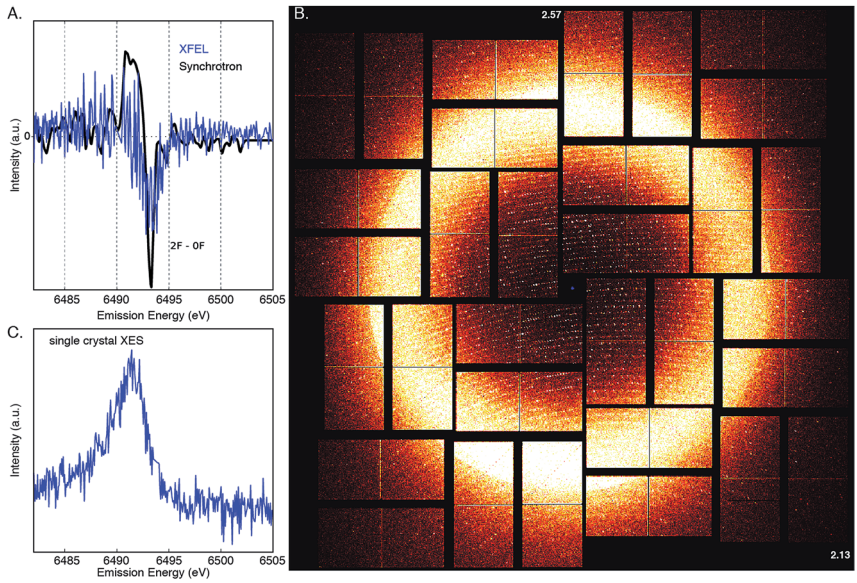

Fig. 4 (A) Overlay of the 2F-dark Mn $K\beta_{1,3}$ XES difference spectra using an XFEL (blue) and a synchrotron (black). (B) fs diffraction pattern of a PS II crystal in the 2 flash state recorded at room temperature, resolution in the corners is 2.13 Å and at the edges 2.57 Å, diffraction spots are visible beyond 2.3 Å resolution. C. Mn $K\beta_{1,3}$ XES from PS II crystals in the 2F state. The spectrum was collected from an experimental run in which 1466 crystal hits were identified in the diffraction detector.

a PS II crystal obtained from injecting a suspension of crystals, with a size distribution of 10–20 micrometers, using an electrofocusing liquid injector with a liquid shield flow (coMESH).[32] An XES spectrum obtained from more than 1400 crystal hits is shown in Fig. 4C, thus providing a diagnostic use of spectroscopy for the chemical state and the intactness of the sample, while collecting XRD data. For XES, each crystal provides only a weak XES signal and accumulation over many individual shots is necessary to obtain an interpretable spectrum for samples like metalloenzymes in which the metal concentration is very low. The characteristics of the individual crystal samples determine the maximum achievable concentration of crystals, and these are often limited by factors like aggregation and sedimentation of the crystals leading to clogging of the injection setup. The necessary reduction of the particle concentration leads then to a lower hit rate, *e.g.* often only a few percent in liquid injector-based crystallography. Therefore the average concentration in the sample volume probed by the X-ray beam is lower, although the intrinsic metal concentration in a protein crystal is generally higher compared to a solution of the same protein. In the case of PS II, the concentration difference between crystals and solution samples is about six times but the hit rate difference is a factor of 20–50. In addition, the jet volume probed by the X-ray beam is not always filled completely by a crystal, giving rise to another reduction in signal level from crystals compared to solution samples. This leads to an average improvement in signal rates for PS II solution samples over crystals by a factor of ~10. In PS II solution samples, with a Mn concentration

of ~1 mM and a path length of 10 micrometers, a total of 600 Mn Kβ fluorescence photons are emitted per shot (40 fs XFEL pulses, 9.5 keV excitation, with 2 mJ per pulse) out of which 8 photons can be theoretically collected by our spectrometer (solid angle of 1.3%).[4] Therefore, the spectroscopic signal needs to be averaged over many shots. In practice, a collection time of 20–30 minutes at 120 Hz X-ray repetition rate for a $K\beta_{1,3}$ spectrum from solutions was necessary to achieve sufficient S/N. To obtain a spectrum of similar quality from a crystal suspension, collection times of 4–5 hours would be necessary. To study the time-evolution of chemical states of the metal cluster, based on small changes in the spectral shape and energy position of the Mn emission, high-quality $K\beta_{1,3}$ XES spectra are required. This is only achievable in a reasonable amount of measurement time with solution samples as they provide a more efficient way of collecting data (100% sample hit rate).

Another point that needs to be taken into account for the simultaneous data collection of diffraction and spectroscopic signal is that both methods are sensitive to different degrees of sample damage. We have shown that XES data, free of electronic damage, can be collected at XFELs together with the XRD data[3,5] under the conditions that were used for these studies (<50 fs pulse duration, spot size of $\sim 1.5 \times 1.5\ \mu m^2$, $3\text{–}6 \times 10^{11}$ photons per pulse at energies between 7 and 9.5 keV, equivalent to an X-ray dose of 50–300 MGy). However, X-ray induced changes to the electronic structure will become visible when the X-ray dose increases (*i.e. via* the increase of incoming X-ray photons/shot, the use of a lower X-ray energy leading to a higher cross section, a better focused beam, *etc.*), and the effect will become noticeable in the XES more easily than in the XRD. Such effects could for example be caused by multiple excitation processes at the same site (either at the same atom or in the same electronically coupled moiety, for example at two neighboring Mn in the Mn_4CaO_5 cluster in PS II). Such effects may not be readily apparent in the diffraction data until the atomic positions are affected, especially as the time scales for electronic and atomic motions are very different. Recent studies, both in the soft- and hard X-ray regime, indicated the onset of such effects under certain conditions, for example in the oxygen K-edge of water,[33] in the Fe L-edge RIXS spectrum of $Fe(CO)_5$ in solution,[34] and in the XRD data of ferredoxin obtained using a very high dose (30 GGy) at the 100 nm focus instrument at CXI, LCLS.[35]

3. Towards studying inorganic electron transfer chromophores

The functionality of metalloenzymes arises as a consequence of the spin state, electronic structure, and ligand environment of the metal catalytic center, cofactor arrangement for electron and proton transfer in both space and time, as well as the pigment–pigment interactions at interfaces. To be useful for driving a multi-electron catalyst, the excited state has to be sufficiently long-lived to allow for electron transport from one pigment/cofactor to another. There are some promising synthetic candidates for this type of photodynamics based on a multimetallic unit anchored on a silica nanoporous surface.[36–40] While the back electron transfer rate and slower changes following the initial MMCT excitation have been studied by various techniques, very little is known about the ultrafast

steps that immediately follow the light excitation. Besides the MMCT there are excited state dynamics, structural rearrangements, and, possibly, spin crossover processes that are critical for the function of these and related systems.

In the case of the TiOMn system ($Ti^{IV}OMn^{II} \rightarrow Ti^{III}OMn^{III}$) (Fig. 5A and B), an excited state lifetime of 1.8 microseconds was established at room temperature (monitored by the dynamics of the ground state MMCT depletion and the Ti^{III} excited state absorption). The unusually slow back electron transfer (k_{BET2}) enables the photocatalytic activity, yet the photochemical yield is determined by competition between two ultrafast processes shown in Fig. 5C, namely ultrafast intersystem crossing (k_{ISC}) *versus* ultrafast back electron transfer in the initially excited S = 5/2 MMCT state (k_{BET1}) following photo excitation. It is the S = 3/2 state with the long lifetime of 1.8 microseconds that gives rise to the observed reactivity. In order to improve and optimize the photocatalytic yield, an understanding of the factors that determine the branching between ultrafast (spin allowed) back electron transfer in the S = 5/2 state *versus* intersystem crossing to the S = 3/2 excited state is essential. Although some of the optical methods can be applied in the femtosecond time regime, the element-specific methods based on X-ray techniques are useful for understanding the local geometric and electronic structure of the metals. At synchrotron radiation sources, X-ray studies have been generally limited to the ~100 ps temporal resolution[41] and therefore XFEL X-ray pulses are required for capturing faster phenomena.

Using wavelength-dispersive XES, we have developed a method to probe multiple elements based on an ultrafast optical pump and X-ray probe to simultaneously detect signals from both metal centers in a time-resolved manner (Fig. 6A and B).[42] The setup, shown in Fig. 6A, allows the time-points to

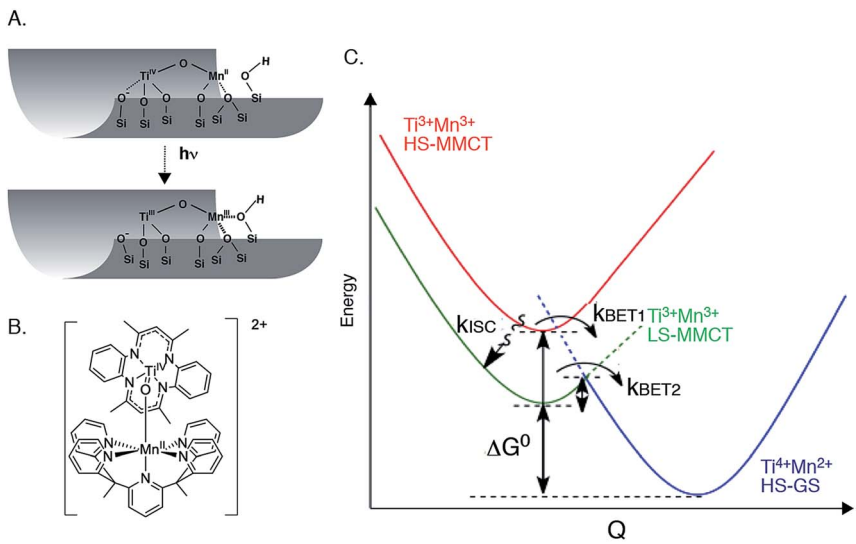

Fig. 5 (A) Schematic of the Ti–O–Mn complex on a mesoporous silica substrate. (B) Structure of a Ti–O–Mn bridged complex. (C) Proposed energy level diagram for the photo-induced metal-to-metal charge transfer (MMCT) processes that determine the photocatalytic yields for the $TiOMn^{II}$ charge transfer unit. k_{BET1} and k_{ISC} are ultrafast, k_{BET2} is the 1.8 μs process.

be accessed within the accuracy of the X-ray jitter and the laser timing. This setup allows the measurement of time-points starting from 300 femtoseconds, which is limited by the accuracy of the timing between the X-ray probe and laser pump.

A multi-crystal von Hamos spectrometer combined with two position-sensitive detectors was used for the data collection of the photo-excitation of

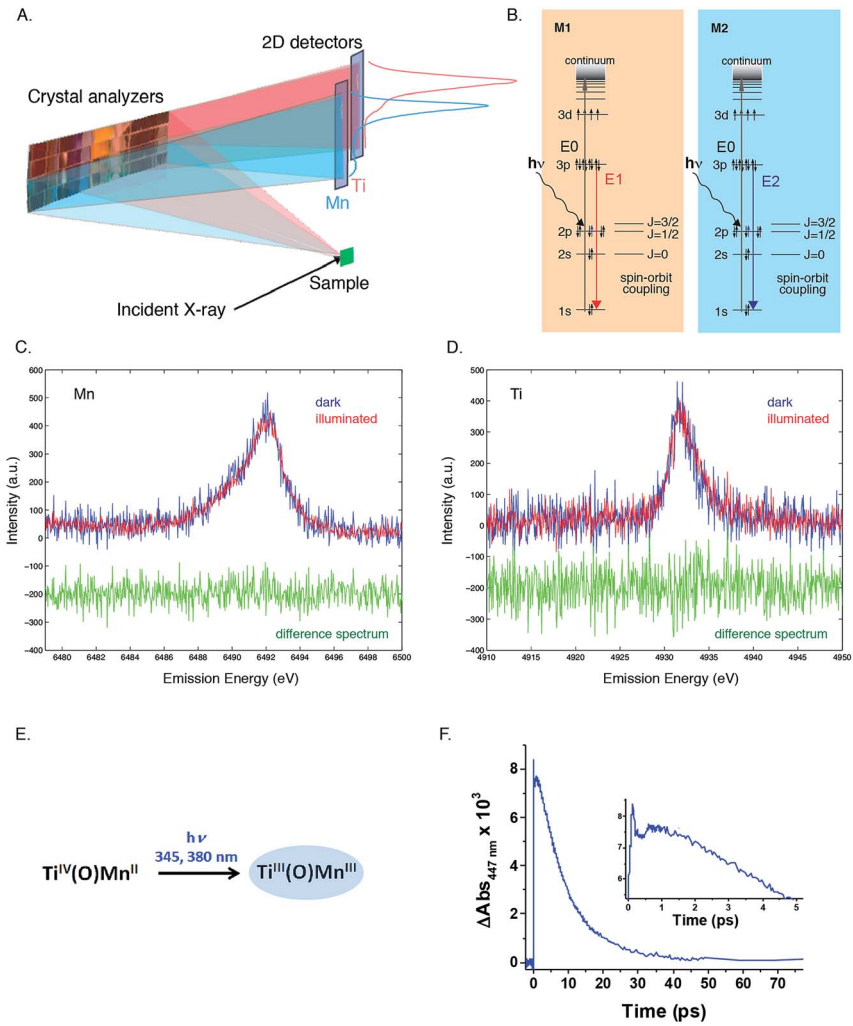

Fig. 6 (A) The schematic shows the method used for the simultaneous collection of the emission spectra from two elements, Mn and Ti, using an energy dispersive X-ray spectrometer and a 2D detector. (B) Energy level diagram showing the excitation, E_1 and E_2, and Kβ emission processes for Mn and Ti. (C) Mn $K\beta_{1,3}$ spectra of the Mn/Ti molecular compound in solution in the dark (blue) and illuminated (1.2 ps) (red). (D) Ti $K\beta_{1,3}$ spectra of the Mn/Ti molecular compound in solution in the dark (blue) and illuminated (1.2 ps) (red). The difference spectra are shown in green. (E) Expected changes of the metal oxidation states during the MMCT. (F) Transient absorption spectroscopy of Mn/Ti molecular compound in solution.

the MnTi system. The data was collected at Hutch 3 in SACLA (SPring-8, Japan), using 7 keV incident X-rays with a pulse duration of ~10 femtoseconds and a beamsize of 50 micrometers. A $Ti^{IV}OMn^{II}$ molecular complex in acetonitrile solution (5 mM Mn and Ti) and a $Ti^{IV}OMn^{II}$ complex anchored to silica nanoparticles (solid) was used for the data collection. The solid sample was mounted on a solid-target stage and was moved to a fresh sample spot shot-by-shot. The liquid sample was injected with a liquid injector (100 μm I.D.). Mn and Ti Kβ emission lines are used to detect the electronic structural changes of the two metal sites simultaneously. Of the 16 slots for cylindrically bent analyzer crystals of the von Hamos spectrometer, eight were populated with Si (440) crystals aligned for the energy range of the Mn Kβ line and the remaining eight with Ge(331) crystals for observing the Ti Kβ line. The Bragg reflections of Mn and Ti Kβ signals from each set of 8 crystals were collected, and focused on the two MPCCD detectors as two separate energy dispersed lines. Prior to the pump–probe experiment, a bismuth crystal was used and its diffraction peak was used to determine the timing between the pump laser and the X-ray laser.

A photon energy above the absorption edges of both elements studied (Ti and Mn, in this case) was used and the metal sites were probed simultaneously by different crystal reflections that disperse the emission signal from each metal onto a separate line on the 2D detectors (Fig. 6A). In this way, the emission signals can be directly correlated on a shot-by-shot basis. This detection scheme circumvents systematic errors induced by the intensity jitter of the XFEL beam, concentration, and volume distribution of the sample. Thus, it results in an efficient way for characterizing ultrafast changes in the local structure of heterometallic active sites where changes in oxidation states occur at either or both metal sites upon light irradiation, such as in the Ti(O)Mn system mentioned above. Studies using this method were conducted on both a Ti-oxo-Mn complex anchored to silica nanoparticles (solid sample) and on a molecular species with the same heterobimetallic core dissolved in a homogeneous solution (liquid sample).[43] Differences in the electron transfer dynamics are expected in the two cases, primarily due to the role played by the nanoparticles *versus* the solvent in stabilizing the species forming along the reaction pathway but also due to kinetic effects induced by the different media. The data for the system anchored to silica nanoparticles showed no change due to electron transfer ~10 ps after optical laser excitation. This suggests that the important charge recombination might occur at the very early stages after laser irradiation of this solid sample. Preliminary UV-Vis transient absorption spectroscopy measurements performed on the liquid sample suggests kinetics that likely corresponds to the oxidation of Mn(II) to Mn(III) (and the reduction of Ti(IV) to Ti(III)) upon optical laser excitation of the initial sample, showing the maximum formation of the product around 1 ps after laser irradiation (Fig. 6E and F). However, data from the pump–probe experiment performed at the SACLA XFEL collected after 1.2 ps does not show clear changes of the metal oxidation states (Fig. 6C and D). Likely reasons for this are the current data quality or the population of the excited state being under the detection limit. More detailed data analysis including shorter delay times is necessary for both the silica-anchored and the Ti(O)Mn liquid samples, and such a study is underway.

4. Conclusion and future direction

We have developed XFEL-based methods for studying the structure of complex biological metalloenzymes and for studying the electronic structural dynamics of both biological and inorganic systems. The simultaneous detection of XRD and XES from metalloenzymes allows the investigation of both the geometric and electronic structure of enzymatic reactions in real time at physiological temperatures, and to ensure the integrity and intermediate state characterization of short-lived intermediate states. The method of simultaneous detection of the X-ray emission spectra from multiple elements after optical excitation has great potential for probing the dynamics of MMCT or charge-separated states where charge transfer occurs on ultrafast time scales. This method will help with understanding the fundamentals that govern multidimensionally (time and space) controlled chemistry, by detecting competing pathways of energy loss and observing energy transfer processes. Femtosecond X-ray spectroscopy is a unique tool that provides access to these insights and can guide design improvements for maximizing branching in favor of the photochemically active charge-separated or MMCT states. The knowledge gained from these studies will not only help the understanding of currently known biochemical processes, but may also lead to the improvement/design of novel catalytic systems.

Besides the various advantages that the use of XFELs has brought to the field of biology and chemistry by using the fs X-ray probes to interrogate ps and sub ps timescales and outrun damage processes that otherwise often hinder X-ray studies at conventional synchrotron sources, there are some limitations to this approach. The most important point is that further increasing the X-ray dose may not help to get the intact form of the XRD and spectroscopic data, due to the limitation that comes from electronic damage to the samples in these high-flux regimes. Instead, increasing the X-ray repetition rate will be a huge advantage, in particular, for spectroscopic data collection at time delays that are large compared to the X-ray and laser timing jitter, as in these cases often it is not necessary to collect shot-by-shot information and the signal can be averaged over many shots without the need of a high repetition rate detection system. Nevertheless, at very high repetition rates, one has to consider the effect of the shock wave created by an X-ray pulse hitting the sample on the neighboring sample volume both in a continuous jet or a stream of droplets (see ref. 44) and high speed sample delivery schemes have to be designed accordingly. Another approach will be to use stimulated X-ray emission processes to enhance the signal intensity. The possibility of a non linear X-ray spectroscopy approach has been postulated theoretically (*e.g.* ref. 45–47) and recently the induction of stimulated emission processes was demonstrated experimentally for neon gas in the soft X-ray regime[48,49] and a Cu foil in the hard X-ray regime.[50] When established, this approach will be truly beneficial for collecting data from dilute samples or less-probable transitions. Whether the stimulated process is applicable to more dilute systems, in which the shot-by-shot spectroscopic information is currently not accessible due to the limited S/N ratio, is still an open question.

Author contributions

Data collection at XFELs LCLS/SACLA – R. A.-M., K. A., U. B., R. C., F. D. F., H. F., D. I., T. Ka., J. F. K., T. Kr., Y. K., K. M., K. N., T. N., C. S., Y. S., T. T., K. U., T.-C. W., V. K. Y., J. Y. Sample injector – J. F. K., C. S., F. D. F., S. G., R. G. S. Emission spectrometer – R.-A. M., U. B., D. S., T.-C. W. SACLA scientific support – T. K., T. T., M. Y. Samples Mn–Ti – W. W. W., E. G., B. A. M., H. M. F. Samples PS II – M. I., A. Z., R. C. Optical spectroscopy – C. S., J. K. C. X-ray emission spectra analysis – T. Kr., F. D. F., K. M. X-ray diffraction data analysis – N. K. S., A. S. B., I. D. Y. Experiment design and writing – T. K., J. F. K., R.-A. M., U. B., H. M. F., W. W. W., K. N., J. M., K. U., M. Y., A. Z., V. K. Y., J. Y.

Acknowledgements

The authors acknowledge research support from the Director, Office of Science, Office of Basic Energy Sciences, Division of Chemical Sciences, Geosciences, and Biosciences of the Department of Energy (DOE) under contract DE-AC02-05CH11231 (J. Y., V. K. Y., and H. F.), the NIH grants GM116423 (F. D. F.), GM55302 (V. K. Y.), GM095887 (N. K. S.), GM102520 (N. K. S.), and GM110501 (J. Y.), and the Human Frontier Research grant RGP0063/2013 (J. Y., U. B., A. Z.). Use of the Linac Coherent Light Source (LCLS), SLAC National Accelerator Laboratory, is supported by the U.S. Department of Energy, Office of Science, Office of Basic Energy Sciences under contract No. DE-AC02-76SF00515. H. F., K. M., K. N. and K. U. acknowledge research support by the X-ray Free Electron Laser Utilization Research Project and the X-ray Free Electron Laser Priority Strategy Program of the Ministry of Education, Culture, Sports, Science and Technology of Japan (MEXT). H. F., K. N. and K. U. are supported by the Japan Society for the Promotion of Science (JSPS), H. F. and K. U. by the IMRAM project, and K. N. by the Cooperative Research Program of the "Network Joint Research Center for Materials and Devices" of Japan. The DFG-Cluster of Excellence "UniCat" coordinated by the Technische Universität Berlin and Sfb1078, TP A5 (A. Z.); the Solar Fuels Strong Research Environment (Umeå University), the Artificial Leaf Project (K&A Wallenberg Foundation 2011.0055) and Energimyndigheten (36648-1) (J. M.) are acknowledged for supporting this project. The Mn/Ti data collection was done at SACLA (Japan), under proposal numbers 2014A8013 and 2015A8007. The transient absorption spectra were taken at the Joint Center for Artificial Photosynthesis (JCAP), DOE Energy Innovation Hub under award no. DE-SC0004993. We are grateful to our present and former group members and all our collaborators, who contributed to the research from our group presented in this review. We especially like to thank the CXI beamline scientists at the LCLS, Sébastien Boutet, Garth Williams, and Mengning Liang and all the CXI support staff. We thank Raymond Sierra, Hartawan Laksmono, and Claudiu Stan for help with the MESH injector. We thank Gabriella Carini, Sven Herrmann, and Jack Pines from LCLS for support with data collection at SACLA. We also thank the excellent support staff at LCLS and SACLA, where the XFEL experiments were conducted and at SSRL (BL 6-2) and ALS (BL 5.0.2), where the synchrotron experiments were conducted.

Notes and references

1 M. Suga, F. Akita, K. Hirata, G. Ueno, H. Murakami, Y. Nakajima, T. Shimizu, K. Yamashita, M. Yamamoto, H. Ago and J. R. Shen, *Nature*, 2015, **517**, 99–103.
2 Y. Umena, K. Kawakami, J. R. Shen and N. Kamiya, *Nature*, 2011, **473**, 55–60.
3 R. Alonso-Mori, J. Kern, R. J. Gildea, D. Sokaras, T. C. Weng, B. Lassalle-Kaiser, R. Tran, J. Hattne, H. Laksmono, J. Hellmich, C. Glockner, N. Echols, R. G. Sierra, D. W. Schafer, J. Sellberg, C. Kenney, R. Herbst, J. Pines, P. Hart, S. Herrmann, R. W. Grosse-Kunstleve, M. J. Latimer, A. R. Fry, M. M. Messerschmidt, A. Miahnahri, M. M. Seibert, P. H. Zwart, W. E. White, P. D. Adams, M. J. Bogan, S. Boutet, G. J. Williams, A. Zouni, J. Messinger, P. Glatzel, N. K. Sauter, V. K. Yachandra, J. Yano and U. Bergmann, *Proc. Natl. Acad. Sci. U. S. A.*, 2012, **109**, 19103–19107.
4 R. Alonso-Mori, J. Kern, D. Sokaras, T. C. Weng, D. Nordlund, R. Tran, P. Montanez, J. Delor, V. K. Yachandra, J. Yano and U. Bergmann, *Rev. Sci. Instrum.*, 2012, **83**, 073114.
5 J. Kern, R. Alonso-Mori, R. Tran, J. Hattne, R. J. Gildea, N. Echols, C. Glockner, J. Hellmich, H. Laksmono, R. G. Sierra, B. Lassalle-Kaiser, S. Koroidov, A. Lampe, G. Y. Han, S. Gul, D. DiFiore, D. Milathianaki, A. R. Fry, A. Miahnahri, D. W. Schafer, M. Messerschmidt, M. M. Seibert, J. E. Koglin, D. Sokaras, T. C. Weng, J. Sellberg, M. J. Latimer, R. W. Grosse-Kunstleve, P. H. Zwart, W. E. White, P. Glatzel, P. D. Adams, M. J. Bogan, G. J. Williams, S. Boutet, J. Messinger, A. Zouni, N. K. Sauter, V. K. Yachandra, U. Bergmann and J. Yano, *Science*, 2013, **340**, 491–495.
6 J. Hattne, N. Echols, R. Tran, J. Kern, R. J. Gildea, A. S. Brewster, R. Alonso-Mori, C. Glockner, J. Hellmich, H. Laksmono, R. G. Sierra, B. Lassalle-Kaiser, A. Lampe, G. Han, S. Gul, D. DiFiore, D. Milathianaki, A. R. Fry, A. Miahnahri, W. E. White, D. W. Schafer, M. M. Seibert, J. E. Koglin, D. Sokaras, T. C. Weng, J. Sellberg, M. J. Latimers, P. Glatzel, P. H. Zwart, R. W. Grosse-Kunstleve, M. J. Bogan, M. Messerschmidt, G. J. Williams, S. Boutet, J. Messinger, A. Zouni, J. Yano, U. Bergmann, V. K. Yachandra, P. D. Adams and N. K. Sauter, *Nat. Methods*, 2014, **11**, 545–548.
7 R. Mitzner, J. Rehanek, J. Kern, S. Gul, J. Hattne, T. Taguchi, R. Alonso-Mori, R. Tran, C. Weniger, H. Schroder, W. Quevedo, H. Laksmono, R. G. Sierra, G. Y. Han, B. Lassalle-Kaiser, S. Koroidov, K. Kubicek, S. Schreck, K. Kunnus, M. Brzhezinskaya, A. Firsov, M. P. Minitti, J. J. Turner, S. Moeller, N. K. Sauter, M. J. Bogan, D. Nordlund, W. F. Schlotter, J. Messinger, A. Borovik, S. Techert, F. M. F. de Groot, A. Fohlisch, A. Erko, U. Bergmann, V. K. Yachandra, P. Wernet and J. Yano, *J. Phys. Chem. Lett.*, 2013, **4**, 3641–3647.
8 R. Alonso-Mori, D. Sokaras, D. L. Zhu, T. Kroll, M. Chollet, Y. P. Feng, J. M. Glownia, J. Kern, H. T. Lemke, D. Nordlund, A. Robert, M. Sikorski, S. Song, T. C. Weng and U. Bergmann, *J. Synchrotron Radiat.*, 2015, **22**, 612–620.
9 B. Kok, B. Forbush and M. Mcgloin, *Photochem. Photobiol.*, 1970, **11**, 457–475.
10 *Photosystem II: The Light-Driven Water: Plastoquinone Oxidoreductase*, ed. T. Wydrzynski and S. Satoh, Springer, Dordrecht, 2005.
11 R. J. Debus, *Coord. Chem. Rev.*, 2008, **252**, 244–258.

12 J. Messinger, T. Noguchi and J. Yano, Photosynthetic O_2 evolution, in *Molecular solar fuels*, ed. T. J. Wydrzynski and W. Hillier, RSC, London, 2012, ch. 7, pp. 163–207.
13 H. N. Chapman, P. Fromme, A. Barty, T. A. White, R. A. Kirian, A. Aquila, M. S. Hunter, J. Schulz, D. P. DePonte, U. Weierstall, R. B. Doak, F. R. N. C. Maia, A. V. Martin, I. Schlichting, L. Lomb, N. Coppola, R. L. Shoeman, S. W. Epp, R. Hartmann, D. Rolles, A. Rudenko, L. Foucar, N. Kimmel, G. Weidenspointner, P. Holl, M. N. Liang, M. Barthelmess, C. Caleman, S. Boutet, M. J. Bogan, J. Krzywinski, C. Bostedt, S. Bajt, L. Gumprecht, B. Rudek, B. Erk, C. Schmidt, A. Homke, C. Reich, D. Pietschner, L. Struder, G. Hauser, H. Gorke, J. Ullrich, S. Herrmann, G. Schaller, F. Schopper, H. Soltau, K. U. Kuhnel, M. Messerschmidt, J. D. Bozek, S. P. Hau-Riege, M. Frank, C. Y. Hampton, R. G. Sierra, D. Starodub, G. J. Williams, J. Hajdu, N. Timneanu, M. M. Seibert, J. Andreasson, A. Rocker, O. Jonsson, M. Svenda, S. Stern, K. Nass, R. Andritschke, C. D. Schroter, F. Krasniqi, M. Bott, K. E. Schmidt, X. Y. Wang, I. Grotjohann, J. M. Holton, T. R. M. Barends, R. Neutze, S. Marchesini, R. Fromme, S. Schorb, D. Rupp, M. Adolph, T. Gorkhover, I. Andersson, H. Hirsemann, G. Potdevin, H. Graafsma, B. Nilsson and J. C. H. Spence, *Nature*, 2011, **470**, 73–U81.
14 E. F. Garman and M. Weik, *J. Synchrotron Radiat.*, 2015, **22**, 195–200.
15 J. Yano, J. Kern, K. D. Irrgang, M. J. Latimer, U. Bergmann, P. Glatzel, Y. Pushkar, J. Biesiadka, B. Loll, K. Sauer, J. Messinger, A. Zouni and V. K. Yachandra, *Proc. Natl. Acad. Sci. U. S. A.*, 2005, **102**, 12047–12052.
16 K. D. Daughtry, Y. Xiao, D. Stoner-Ma, E. Cho, A. M. Orville, P. Liu and K. N. Allen, *J. Am. Chem. Soc.*, 2012, **134**, 2823–2834.
17 K. G. Sigfridsson, P. Chernev, N. Leidel, A. Popovic-Bijelic, A. Graslund and M. Haumann, *J. Biol. Chem.*, 2013, **288**, 9648–9661.
18 J. S. Fraser, H. van den Bedem, A. J. Samelson, P. T. Lang, J. M. Holton, N. Echols and T. Alber, *Proc. Natl. Acad. Sci. U. S. A.*, 2011, **108**, 16247–16252.
19 D. H. Juers and B. W. Matthews, *J. Mol. Biol.*, 2001, **311**, 851–862.
20 R. F. Tilton, J. C. Dewan and G. A. Petsko, *Biochemistry*, 1992, **31**, 2469–2481.
21 S. Boutet and G. J. Williams, *New J. Phys.*, 2010, **12**, 035024.
22 M. N. Liang, G. J. Williams, M. Messerschmidt, M. M. Seibert, P. A. Montanez, M. Hayes, D. Milathianaki, A. Aquila, M. S. Hunter, J. E. Koglin, D. W. Schafer, S. Guillet, A. Busse, R. Bergan, W. Olson, K. Fox, N. Stewart, R. Curtis, A. A. Miahnahri and S. Boutet, *J. Synchrotron Radiat.*, 2015, **22**, 514–519.
23 J. Kern, R. Tran, R. Alonso-Mori, S. Koroidov, N. Echols, J. Hattne, M. Ibrahim, S. Gul, H. Laksmono, R. G. Sierra, R. J. Gildea, G. Han, J. Hellmich, B. Lassalle-Kaiser, R. Chatterjee, A. S. Brewster, C. A. Stan, C. Glockner, A. Lampe, D. DiFiore, D. Milathianaki, A. R. Fry, M. M. Seibert, J. E. Koglin, E. Gallo, J. Uhlig, D. Sokaras, T. C. Weng, P. H. Zwart, D. E. Skinner, M. J. Bogan, M. Messerschmidt, P. Glatzel, G. J. Williams, S. Boutet, P. D. Adams, A. Zouni, J. Messinger, N. K. Sauter, U. Bergmann, J. Yano and V. K. Yachandra, *Nat. Commun.*, 2014, **5**, 4371.
24 G. Renger, *Physiol. Plant.*, 1997, **100**, 828–841.
25 M. R. Razeghifard and R. J. Pace, *Biochim. Biophys. Acta, Bioenerg.*, 1997, **1322**, 141–150.

26 M. Haumann, P. Liebisch, C. Muller, M. Barra, M. Grabolle and H. Dau, *Science*, 2005, **310**, 1019–1021.
27 H. J. Eckert and G. Renger, *Photochem. Photobiol.*, 1980, **31**, 501–511.
28 R. Krivanek, J. Kern, A. Zouni, H. Dau and M. Haumann, *Biochim. Biophys. Acta, Bioenerg.*, 2007, **1767**, 520–527.
29 A. Guskov, A. Gabdulkhakov, M. Broser, J. Kern, A. Zouni and W. Saenger, *J. Biomol. Struct. Dyn.*, 2009, **26**, 865.
30 R. de Wijn and H. J. van Gorkom, *Biochemistry*, 2001, **40**, 11912–11922.
31 G. Ananyev and G. C. Dismukes, *Photosynth. Res.*, 2005, **84**, 355–365.
32 R. G. Sierra, C. Gati, H. Laksmono, E. H. Dao, S. Gul, F. Fuller, J. Kern, R. Chatterjee, M. Ibrahim, A. S. Brewster, I. D. Young, T. Michels-Clark, A. Aquila, M. Liang, M. S. Hunter, J. E. Koglin, S. Boutet, E. A. Junco, B. Hayes, M. J. Bogan, C. Y. Hampton, E. V. Puglisi, N. K. Sauter, C. A. Stan, A. Zouni, J. Yano, V. K. Yachandra, S. M. Soltis, J. D. Puglisi and H. DeMirci, *Nat. Methods*, 2016, **13**, 59–62.
33 S. Schreck, M. Beye, J. A. Sellberg, T. McQueen, H. Laksmono, B. Kennedy, S. Eckert, D. Schlesinger, D. Nordlund, H. Ogasawara, R. G. Sierra, V. H. Segtnan, K. Kubicek, W. F. Schlotter, G. L. Dakovski, S. P. Moeller, U. Bergmann, S. Techert, L. G. M. Pettersson, P. Wernet, M. J. Bogan, Y. Harada, A. Nilsson and A. Föhlisch, *Phys. Rev. Lett.*, 2014, **113**, 153002.
34 P. Wernet, K. Kunnus, I. Josefsson, I. Rajkovic, W. Quevedo, M. Beye, S. Schreck, S. Grubel, M. Scholz, D. Nordlund, W. Zhang, R. W. Hartsock, W. F. Schlotter, J. J. Turner, B. Kennedy, F. Hennies, F. M. de Groot, K. J. Gaffney, S. Techert, M. Odelius and A. Fohlisch, *Nature*, 2015, **520**, 78–81.
35 K. Nass, L. Foucar, T. R. Barends, E. Hartmann, S. Botha, R. L. Shoeman, R. B. Doak, R. Alonso-Mori, A. Aquila, S. Bajt, A. Barty, R. Bean, K. R. Beyerlein, M. Bublitz, N. Drachmann, J. Gregersen, H. O. Jonsson, W. Kabsch, S. Kassemeyer, J. E. Koglin, M. Krumrey, D. Mattle, M. Messerschmidt, P. Nissen, L. Reinhard, O. Sitsel, D. Sokaras, G. J. Williams, S. Hau-Riege, N. Timneanu, C. Caleman, H. N. Chapman, S. Boutet and I. Schlichting, *J. Synchrotron Radiat.*, 2015, **22**, 225–238.
36 H. Frei, *Chimia*, 2009, **63**, 721–730.
37 H. S. Soo, M. L. Macnaughtan, W. W. Weare, J. Yano and H. Frei, *J. Phys. Chem. C*, 2011, **115**, 24893–24905.
38 X. N. Wu, W. W. Weare and H. Frei, *Dalton Trans.*, 2009, 10114.
39 B. A. McClure and H. Frei, *J. Phys. Chem. C*, 2014, **118**, 11601–11611.
40 W. Kim, B. A. McClure, E. Edri and H. Frei, *Chem. Soc. Rev.*, 2016, **45**, 3221–3243.
41 G. Vanko, P. Glatzel, V. T. Pham, R. Abela, D. Grolimund, C. N. Borca, S. L. Johnson, C. J. Milne and C. Bressler, *Angew. Chem., Int. Ed.*, 2010, **49**, 5910–5912.
42 S. Gul, J. W. D. Ng, R. Alonso-Mori, J. Kern, D. Sokaras, E. Anzenberg, B. Lassalle-Kaiser, Y. Gorlin, T.-C. Weng, P. H. Zwart, J. Z. Zhang, U. Bergmann, V. K. Yachandra, T. F. Jaramillo and J. Yano, *Phys. Chem. Chem. Phys.*, 2015, **17**, 8901–8912.
43 E. M. Goggins, T. T. Lekich, W. W. Weare, R. D. Sommer, M. A. Ribeiro and C. B. Pinheiro, *Eur. J. Inorg. Chem.*, 2016, **2016**, 1054–1059.
44 C. A. Stan, D. Milathianaki, H. Laksmono, R. G. Sierra, T. A. McQueen, M. Messerschmidt, G. J. Williams, J. E. Koglin, T. J. Lane, M. J. Hayes,

S. A. H. Guillet, M. Liang, A. L. Aquila, P. R. Willmott, J. S. Robinson, K. L. Gumerlock, S. Botha, K. Nass, I. Schlichting, R. L. Shoeman, H. A. Stone and S. Boutet, *Nat. Phys.*, 2016, DOI: 10.1038/nphys3779.

45 S. Tanaka and S. Mukamel, *Phys. Rev. Lett.*, 2002, **89**, 043001.

46 V. Kimberg and N. Rohringer, *Phys. Rev. Lett.*, 2013, **110**, 043901.

47 Y. Zhang, J. D. Biggs and S. Mukamel, *ChemPhysChem*, 2015, **16**, 2006–2014.

48 N. Rohringer, D. Ryan, R. A. London, M. Purvis, F. Albert, J. Dunn, J. D. Bozek, C. Bostedt, A. Graf, R. Hill, S. P. Hau-Riege and J. J. Rocca, *Nature*, 2012, **481**, 488–491.

49 C. Weninger, M. Purvis, D. Ryan, R. A. London, J. D. Bozek, C. Bostedt, A. Graf, G. Brown, J. J. Rocca and N. Rohringer, *Phys. Rev. Lett.*, 2013, **111**, 233902.

50 H. Yoneda, Y. Inubushi, K. Nagamine, Y. Michine, H. Ohashi, H. Yumoto, K. Yamauchi, H. Mimura, H. Kitamura, T. Katayama, T. Ishikawa and M. Yabashi, *Nature*, 2015, **524**, 446–449.

